Star formation and the interstellar medium in galaxy simulations

Gerritsen, Jeroen Peter Erik

2

Star Formation in N-body simulations

J.P.E. Gerritsen & V. Icke

We present numerical simulations of isolated disk galaxies including gas dynamics and star formation. The gas is allowed to cool to 10 K, while heating of the gas is provided by the far-ultraviolet flux of all stars. Stars are allowed to form from the gas according to a Jeans instability criterion: gas is unstable when the Jeans mass is smaller than a critical mass, and stars form as soon as the gas remains unstable longer than the collapse time. With these ingredients we are able to create a two-phase interstellar medium (ISM) and our model gives realistic star formation rates (SFRs).

We investigate the influence of free parameters on the star formation. In order of decreasing importance these are: ionization fraction of the gas (determines the cooling properties), initial mass function (controls the heat input for the gas), collapse time for molecular clouds, and star formation efficiency.

In the simulations the star formation quickly settles a kind of thermal equilibrium of the ISM. This result strongly favours the self-regulating mechanism for star formation.

The model yields a Schmidt law power dependence of the SFR on gas density (SFR $\propto \rho^n$) with index $n \approx 1.3$, in good agreement with observations.

The simulations show that star formation can only occur in the mid-plane of the galaxy, where the gas is dense enough to cool below 100 K. The gas above the plane and outside approximately 6 radial scale lengths is always warm ($T > 8000$ K), heated by the stellar photons. It suggests that radial truncation of stellar disks is a thermal rather than a dynamical process.

Flocculent spiral structure is generally found in the cold gas and consequently also in the young stellar population. It suggests that flocculent spirals are due to the dissipational nature of gas.

ASSIDUOUS study of spiral galaxies has not yet led to a detailed understanding of their structure, formation and evolution. In particular the physics regulating the formation of stars, and the connection to the global properties of galaxies, is poorly understood. From small scale studies we know that stars form in cold molecular clouds with temperatures below 100 K, but what process is governing the large scale star formation is not clear.

In the last few years several studies have put observational constraints on models of star formation. Kennicutt (1983, 1989) measured the Hα flux (which is believed to be a measure of the current star formation rate (SFR) of stars with masses in excess of 10 $M_\odot$) for a large sample of spiral galaxies and found a dependence of the SFR on the total gas density that is well described by a power law with index $n = 1.3 \pm 0.3$. Recently Ryder & Dopita (1994) obtained photometric CCD imaging data for 34 spiral galaxies. From their I, V and Hα images, they find a correlation between the surface brightness in the I-band (supposed to measure the surface density of the old, low-mass stars) and the Hα band. Their conclusion is that the stellar distribution largely controls the SFR and hence

the mass distribution.

The theoretical understanding of star formation on large scales and galaxy evolution in general is still in its infancy. The problem is that a wide range of physical processes is involved: gravitational dynamics, hydrodynamics, gas heating and cooling, and stellar evolution. Since all these processes are intimately related, the subject is awfully complicated, and is very hard to tackle analytically. Therefore, at this moment, numerical techniques provide the best possibilities of studying galaxy evolution. Especially the development of N-body codes using a hierarchical tree structure (e.g. Barnes & Hut 1986; Hernquist 1987) is very promising as it does not place any restrictions on spatial resolution or geometry, and the computing time scales only as $O(N \log N)$. The Lagrangian approach of smoothed particle hydrodynamics (SPH; Lucy 1977; Gingold & Monaghan 1977) allows a straightforward inclusion into N-body algorithms. A successful merger of a tree code with an SPH code is TREESPH (Hernquist & Katz 1989), which has been used to study the evolution of galaxy mergers (e.g. Barnes & Hernquist 1991; Mihos & Hernquist 1994) and the formation of galaxies (Katz & Gunn 1991; Katz 1992).

The next step is a proper description of star formation in these numerical codes. The inclusion of star formation is difficult for various reasons, both numerical and theoretical. First of all, the physics governing star formation is not well understood. This means that a description of star formation in numerical codes must either be based on simple gravitational instability considerations or must rely on an observational star formation "law" from disk galaxies, where one has to assume that the same law holds in other circumstances.

Second, there is a gap of a factor 10^7 or so between the size of a galaxy and that of a protostar globule. Since computing time scales as the third power of spatial resolution, this gap will never be bridged. Therefore we must make plausibility arguments for all unresolved processes. Each of the consequent assumptions is a legitimate target for criticism. We try to minimise the damage by choosing star formation criteria that are based on global properties, and thereby maintain a link between the behaviour of the galaxy as a whole and the unresolved small-scale processes. In particular – and we see this as one of our main improvements – our star formation recipe uses a Jeans criterion for the gas as a whole, supplemented with an estimate of the cloud collapse timescale. Thus we forge a connection between the parent galaxy and its small subclouds. In the same vein we calculate cloud heating due to the global radiation field.

Third, there is the computational task of converting gas into stars, which implies many new particles (e.g. Katz 1992; Navarro & White 1993). A sophisticated method has been developed by Mihos & Hernquist (1994), in which gas particles evolve into *hybrid* gas/star particles and finally into stars, thus keeping the total amount of particles fixed, and yet without constraints on mass conversion from gas to stars. A drawback of their model is that the new star and its parent gas particle are kinematically coupled until the gas is entirely depleted.

An important point of concern is the implementation of radiative heating and cooling processes. Often gas is treated as an isothermal gas. An early attempt to create a truly multi-phase medium is given by Hernquist (1989). Recently, Katz, Weinberg & Hernquist (1996) expanded on previous work and solve for the ionization equilibrium with an ultraviolet radiation background. However in all these models gas is not allowed to cool radiatively below 10^4 K (cooling to low temperatures by adiabatic expansion is often allowed), while we know from observations that stars are formed in cold, molecular clouds with temperatures below 100 K.

In order to improve upon this situation, we developed an algorithm in which the gas is heated by the radiation from *all* stars. The resulting radiation field is position and time de-

pendent, since we follow stellar associations during their evolution. The gas is allowed to have temperatures between 10 and 10^6 K, although these high temperatures are never reached (we do not yet include supernovae that could produce them). We use a Jeans instability condition to localize star forming regions, and scale the collapse time for an unstable region directly to the free-fall time. A stellar cluster is formed as soon as the region is unstable longer than the collapse time. In this way we have constructed a self-consistent model where heating and cooling are intimately coupled and direct feedback from star formation is insured. The one major deficiency is that we do not solve the equations of radiative transfer; heating photons are assumed to percolate throughout the galaxy.

In this paper we discuss the importance of a variety of parameters on the outcome of our simulations, and explore some interesting consequences thereof. In §2.1 we give a detailed description of the star forming algorithm. We explore the parameter space in §2.2.2 using a model for NGC6503. A detailed analysis of the spatial effects of star formation and the two-phase ISM is given in §2.2.3. In §2.3 we interpret our results as self-regulating star formation and we provide a physical basis for stochastic star formation and galaxy truncation.

2.1 Numerical technique

We model the evolution of galaxies using a hybrid N-body/hydrodynamics code (TREESPH; Hernquist & Katz 1989). A brief summary of the techniques pioneered by these authors follows. A tree algorithm (Barnes & Hut 1986; Hernquist 1987) determines the gravitational forces on the collisionless and gaseous components of the galaxies. The hydrodynamic properties of the gas are modeled using SPH. The gas evolves according to hydrodynamic conservation laws, including an artificial viscosity for an accurate treatment of shocks. Each particle is assigned an individual smoothing length, h_i, which determines the local resolution and an individual time step. Estimates of the gas properties are found by smoothing over 32 neighbours within $2h$. We adopt the equation of state

$$P = (\gamma - 1)\rho u, \tag{2.1}$$

where P is the pressure, ρ the density, u the thermal energy density, and $\gamma = 5/3$ for an ideal gas. In the Lagrangian formulation of SPH energy conservation can be expressed as

$$\frac{du}{dt} = -\frac{P}{\rho}\nabla\vec{v} + (\Gamma - \rho\Lambda), \tag{2.2}$$

where $\vec{v}$ is the velocity, and $(\Gamma - \rho\Lambda)$ represents the energy sources and sinks.

The cooling term $\rho\Lambda$ in Eq.(2.2) describes radiative cooling of the gas and is sensitive to the chemical abundances. We do not alter this composition, but instead we assume a hydrogen gas mix with a helium mass fraction of 0.25. For this "standard" gas, cooling functions can be found in the literature (e.g. Dalgarno & McCray 1972). We parametrize the cooling function as

$$\begin{aligned}\Lambda &= 1.0\times10^{-21}\, n_{\rm H}^2[10^{-0.1-1.88(5.23-\log T)^4} + \\ &\quad 1.0\times10^{-a-b(4-\log T)^2}]\ \text{ergs cm}^{-3}\ \text{s}^{-1}, \\ &\quad \text{if } \log T \le 6.2\end{aligned} \tag{2.3}$$

and

$$\begin{aligned}\Lambda &= 1.0\times10^{-22.7}\, n_{\rm H}^2\ \text{ergs cm}^{-3}\ \text{s}^{-1}, \\ &\quad \text{if } \log T > 6.2,\end{aligned} \tag{2.4}$$

where T is the temperature in Kelvin. The second term on the right hand side of Eq.(2.3) determines the cooling below 10^4 K. This part of the cooling function is strongly dependent on the ionization parameter $x = n_e/n_{\rm H}$. We parametrize this part of the cooling function with a and b. Values can be found in Table 2.1. Since we do not solve the ionization balance, we choose the ionization parameter *a priori*.

The largest contributor to the gas heating Γ is photoelectric heating of small grains and PAHs (see e.g. Wolfire et al. 1995). The heating rate is given by

$$\Gamma = 1.0\times10^{-24}\,\epsilon G_0\ \text{ergs}\ \text{s}^{-1}, \tag{2.5}$$

TABLE 2.1— Cooling function parameters a, b for various ionization parameters x.

$\log x$	a	b
-1	3.24	0.170
-2	4.06	0.190
-3	4.40	0.250
-4	4.43	0.273

where ϵ is the heating efficiency and G_0 is the incident far-ultraviolet (FUV) field (91.2 nm to 210 nm) normalized to Habing's (1968) estimate of the local interstellar value ($= 1.6 \times 10^{-3}$ ergs cm^{-2} s^{-1}). The heating efficiency $\epsilon \simeq 0.05$ for temperatures below 10000 K. Since at about 10^4 K the cooling increases more than a factor 10^3, this temperature is effectively an upper limit to the gas temperature, virtually independent of the heat input.

During the simulations the cooling time in some regions can become much shorter than the SPH time step, which is determined by the Courant-Friedrichs-Levy (CFL) condition. If the cooling time is very short the gas will reach thermal equilibrium within the SPH time step. Therefore, in those regions where $\Delta t_c < 0.1\Delta t_{\rm CFL}$ we enforce thermal equilibrium by requiring $\Gamma = \rho\Lambda$ and choose as time step $\Delta t = \Delta t_{\rm CFL}$. In other regions we choose as particle time step $\Delta t = \min(\Delta t_{\rm CFL}, \Delta t_c)$. For these latter particles we do not allow a particle to lose more than half its thermal energy in one time step (Katz & Gunn 1991).

Since the gas is heated mainly due to FUV photons, we must calculate the stellar radiation field. Due to the limited resolution of our simulations each star represents a stellar association. Such an association will be called a *star particle*, which we assume to be formed instantaneously. That means that all star particles have an age, but these ages differ from particle to particle. We can attribute to each particle an FUV flux according to its age. For this we constructed look-up tables with FUV fluxes using the population synthesis models of Bruzual & Charlot (1993). The FUV flux is dependent on the initial mass function (IMF) of the stellar cluster and on the lower and upper mass limits of the IMF. Once we have adopted a specific IMF with mass limits, we can calculate the FUV radiation field by summing the FUV fluxes from all stars, corrected for geometrical dilution but not for extinction. The stellar FUV fluxes inside the smoothing length are softened using the spline-kernel which is also used for softening the acceleration (Hernquist & Katz 1989).

A single dynamical particle thus represents an entire stellar association. We suppose that this does not invalidate our models as long as the dynamical disintegration of the association takes more time than the main sequence lifetime of its massive members, which contribute most to the heating flux. This condition is normally fulfilled for the usual stellar mass functions.

Extinction is probably not very important below a hydrogen column density $N \approx 1.2 \times 10^{21}$ cm^{-2} (Wolfire et al. 1995). As an approximation we can model the extinction as exponential decay with distance ($\exp(-\alpha R)$), where $1/\alpha$ is an absorption coefficient. Unless otherwise stated we will take $\alpha = 0$ in our calculations, which produces a transparent ISM.

2.1.1 From ISM to stars and back

Star formation is governed by the delicate symbiosis between stars and the interstellar medium. Stars influence the ISM by heating it, due to FUV-radiation, stellar winds and supernovae, while the ISM in return provides the necessary material to form stars. In this section we give a rough description of star formation and the (local) ISM.

The local ISM consists of several components: hot intercloud medium (10^5 K), H II (10^4 K), warm intercloud medium (8000 K), warm H I (8000 K), H I clouds ($10 - 100$ K) and molecular clouds ($5 - 30$ K). The hot and warm intercloud medium occupy almost 100% of the volume, equally divided. On the other hand, the H I and H_2 clouds contain about 90% of the mass, with the other 10% in the warm intercloud medium (Knapp 1990).

The hot gas is probably heated by supernova shocks, whereas the warm and cold H I and H_2 clouds are heated mainly by the photoelectric ejection of electrons from dust grains by the interstellar radiation field (Wolfire et al. 1995).

Star formation occurs in giant molecular clouds (GMCs). These typically have masses of a few $10^5 - 10^6\ M_\odot$, temperatures around 10 K and number densities in excess of 10^3 cm^{-3} (e.g. Shu, Adams & Lizano 1987; Bodenheimer 1992). GMCs do not collapse as a whole, but fritter away as smaller subclouds inside contract to form stars. Most stars form in associations containing on the order of $10^4\ M_\odot$ of stars. The collapse time is some 10 times the free-fall time, because the clouds cannot dissipate their internal energy fast enough to collapse at their free-fall rates (Elmegreen 1992). The lifetimes of molecular clouds range from 10^7 yr for GMCs to over 10^8 yr for dwarf molecular clouds (Shu, Adams & Lizano 1987.

The formation of stellar associations inside a GMC destroys the cloud within 10 Myr, due to FUV radiation, stellar winds and supernovae (Blaauw 1991). This behaviour is reflected in the star formation efficiency. On the scale of stellar associations the efficiency may be as high as 50%, while for GMCs it is only a few percent (Bodenheimer 1992).

2.1.2 From ISM to stars numerically

The amount of physics in our simulations is limited by the number of particles our computers can handle, which is far smaller than the number of stars and gas clouds in galaxies. We think that the most interesting gas phases for star formation are the warm and cold phases ($10 - 10^4$ K), while the hot phase is of less importance for controlling the star-gas life cycle. The cooling is described by a standard cooling function between $10 - 10^6$ K (Dalgarno & McCray 1972). We do not solve the ionization balance in detail, so we cannot distinguish between cold neutral or molecular gas, and warm neutral and fully ionized gas.

Since photoelectric emission from dust is the most important heating source for the cold and warm gas, we have to calculate the stellar FUV radiation field. A star particle in our simulations corresponds to a *stellar cluster*, with a given IMF and age. Thus we do not form individual stars, but only associations. If the stellar FUV radiation is included, a direct feedback from new star particles upon the ambient gas particles is assured.

Another important feedback of star formation on the ISM is the energy injection into the ISM by supernovae and stellar winds from massive stars. Numerical studies conducted by others have so far concentrated on the feedback from supernovae (and ignored radiative energy input from stars). This supernova energy has been modeled as thermal or mechanical energy input. If it is modeled (partly) as thermal energy, all studies agree that there is little effect on the evolution of the system since the energy is rapidly radiated away (Katz 1992; Navarro & White 1993; Friedli & Benz 1995). This is due to the cooling properties of the gas, which limit the gas to $\lesssim 10^4$ K. If no cooling below this temperature is allowed, then the thermal energy input indeed cannot have a large effect on the evolution. Modeling the supernova energy as mechanical energy poses other problems: only a small fraction can be converted into kinetic energy of surrounding gas particles, otherwise even normal galaxies would expel much of the gas (Mihos & Hernquist 1994; Friedli & Benz 1995). Given the problems involved with incorporating supernova energy, and since we are not trying to model the hot gas and do not return mass from stars to the surrounding ISM, we do not include supernova energy in the present study, although it will be included in future work. In this article however, we focus on the effects of the stellar heating on star formation.

In SPH simulations the particles sample gas properties such as density and temperature. These particles cannot be correctly interpreted as gas clouds: only *groups* of particles

can be considered as clouds. Bearing this in mind we adopted the following recipe for star formation. For each particle, we calculate the Jeans mass

$$M_J = \frac{1}{6}\pi\rho\left(\frac{\pi s^2}{G\rho}\right)^{\frac{3}{2}}, \quad (2.6)$$

(e.g. Binney & Tremaine 1987) where s is the sound speed of the gas and G the gravitational constant. If this quantity is smaller than the mass of a GMC the particle is in a cold, dense environment, resembling a GMC and we declare the particle to be part of a (gravitationally) unstable cloud. Once a region is labeled unstable, it is allowed to form star clusters. The first condition for an SPH particle to form stars can thus be summarized as:

$$M_J < M_c, \quad (2.7)$$

where the critical cloud mass M_c is set a priori and does not change during the simulations (see also section 2.2.2).

Once a region is unstable, it takes a collapse time to form a stellar cluster. This collapse time is the most influential model parameter in our recipe and its value is uncertain. The problem is mainly numerical. We know that subunits inside GMCs exist, where densities reach values exceeding a few 100 cm^{-3} and temperatures fall below a few times 10 K. Especially these high densities are beyond the dynamical range of the present simulations. Moreover new physics is involved in forming these high densities, in particular the self-shielding of molecular clouds (e.g. Van Dishoeck & Black 1986). In these subunits the collapse time is governed by the dissipation time scale which we cannot estimate due to the problems mentioned above. Given all these uncertainties we couple the collapse time simply to the free-fall time. In practice this leads to collapse times of $10^7 - 10^8$ yr, which corresponds to the lifetimes for molecular clouds. In order to have some handle on the collapse time t_c, we introduce a scale parameter f_c,

$$t_c = f_c \times t_{ff} = \frac{f_c}{\sqrt{4\pi G\rho}}. \quad (2.8)$$

The second condition for an SPH particle to form stars can now be stated as:

$$t_u > t_c, \quad (2.9)$$

where t_u is the time that the particle remains in an unstable cloud.

As soon as an SPH particle has fulfilled both conditions (Eq.(2.7) and Eq.(2.9)) part of its mass is converted into a star particle of mass

$$M_* = \epsilon_{\rm SF} M_c, \quad (2.10)$$

where $\epsilon_{\rm SF}$ is the star formation efficiency (SFE). We fix this efficiency at the beginning of the simulation, so that all new star particles have the same mass since M_c does not change. The star particle gets the same IMF as all other star particles, and age zero. New star particles are then included in the calculation of the radiation field; their emission evolves in time according to standard stellar evolution.

To prohibit infinitely low-mass particles we put a lower limit to the minimum mass of a particle, $M_p \geq 0.1 M_{\rm SPH}$, where $M_{\rm SPH}$ is the initial mass of an SPH particle. If the mass of a gas particle falls below this limit when forming a star particle, it is totally converted into stars.

The new star particle gets initial velocity and acceleration equal to that of the parent gas particle; its position is offset in a random direction by an amount $s\Delta t$.

In summary, we devised the following recipe. From our SPH particle distribution we select conglomerates where the Jeans mass is sufficiently below the aggregate mass. We take this to mean that such regions resemble GMCs. We follow them during their dynamical and thermal evolution and if an SPH particle resides in such a region longer than the collapse time, part of its mass is converted into a star particle. This star particle then heats the surrounding gas as its stellar population evolves, possibly inhibiting further star formation.

In this way we have tried to minimise the damage due to the inevitable lack of resolution by choosing star formation criteria that

are based on *global* properties. Our recipe uses a Jeans criterion for the gas as a whole, supplemented with an estimate of the cloud collapse timescale. Thus we forge a connection between the parent galaxy and its unresolved constituents. In the same vein we calculate cloud heating due to the global radiation field. Accordingly, even though an SPH 'neighbourhood' consists of 32 gas particles, we can still pick a much smaller value (such as 10 SPH masses) as the critical cloud mass. We do not thereby claim that this mass scale is resolved (it isn't), but merely maintain that only a small fraction forms stars. This is completely in keeping with the prevailing view that star formation is a stochastic process when seen from the large-scale perspective. All the same it remains true that these assertions must be verified numerically by charting the influence of the choices of various parameters, which indeed we try to do.

2.2 Results

There are many parameters in our model that can be changed: IMF with its mass limits, ionization parameter, cloud mass M_c, collapse time, star formation efficiency, and the number of particles. To obtain an estimate of the relative importance of these parameters, and of the sensitivity of our computations to these values, we tested them with a model for NGC6503 (see Bottema 1993 and Bottema & Gerritsen 1997). This is an Sc galaxy with a maximum rotation velocity of 120 km/s, star formation taking place all over the disk, and a global SFR of about 0.4 $M_\odot$/yr (Kennicutt 1983).

2.2.1 Model galaxy

We assume an exponential stellar disk with an isothermal z-distribution (e.g. Van der Kruit & Searle 1982):

$$\rho(R,z) = \rho_0 \exp(-R/h_*)\,\mathrm{sech}^2(z/z_0), \quad (2.11)$$

with measured radial scale length $h_* = 1.16$ kpc and vertical scale height $z_0 = h_*/6 = 0.19$ kpc. The disk is truncated at 5 scale lengths (5.8 kpc).

The mass of the stellar disk is calculated from the measured stellar velocity dispersions (Bottema 1989) assuming that the z-dispersion, σ_z is due to the surface density of the stellar disk (Σ_*):

$$\sigma_z = \sqrt{\pi G z_0 \Sigma_*}. \quad (2.12)$$

This implies a stability parameter $Q \geq 1.7$ throughout most of the disk, and yields $M_* = 3.49 \times 10^9\ M_\odot$.

Particles are distributed according to the density distribution (Eq. 2.11), and velocities are assigned according to the (gas) rotation curve (with a maximum of 120 km/s) corrected for asymmetric drift. Dispersions in R, z, θ directions are drawn from gaussian distributions with dispersions of $\sigma_R, \sigma_z, \sigma_\theta$ respectively, using the relations

$$\sigma_z = 0.6\,\sigma_R, \quad \sigma_\theta = \frac{\kappa}{2\omega}\sigma_R, \quad (2.13)$$

with ω and κ the orbital and epicyclic frequencies respectively.

The gas surface density distribution is modeled after the H I distribution,

$$\Sigma_g = \Sigma_0(1 - R/h_g), \quad (2.14)$$

with central surface density $\Sigma_0 = 10\ M_\odot/\mathrm{pc}^2$, and radial extension $h_g = 14.5$ kpc. In our calculations we truncate the gas distribution at 8 kpc, well outside the stellar disk, to save computing time. This yields a total gas mass $1.26 \times 10^9\ M_\odot$. Gas particle velocities are initiated according to the rotation curve. Dispersions are drawn from gaussian distributions, adopting an isotropic dispersion of 6 km/s.

A halo is included in the calculations as a rigid potential. This is justified since the galaxy evolves in isolation. As advantages we do not have to make assumptions about halo particle orbits, and we do not have to spend time in calculating the force of the halo particles on the galaxy. We assign an isothermal density distribution to the halo,

$$\rho_h = \frac{\rho_0}{1 + (r/r_c)^2}, \quad (2.15)$$

with central volume density $\rho_0 = 0.582\ M_\odot/\mathrm{pc}^3$ and core radius $r_c = 624$ pc.

This will correctly put the maximum rotation velocity at 120 km/s.

2.2.2 Parameter space

The influence of the model parameters on global parameters such as the star formation rate and cold gas fraction is tested by changing one parameter compared to a standard setting. The default setting is as follows:

$$\begin{aligned} N_{\rm SPH} &= 5000 \\ N_* &= 10000 \\ M_c &= 2.5 \times 10^6\ M_\odot \\ t_c &= t_{ff} \\ \epsilon_{\rm SF} &= 0.1 \\ x &= 0.1 \\ \alpha &= 0 \end{aligned} \qquad (2.16)$$

We use a Salpeter IMF with $M_{\rm low} = 0.1$ and $M_{\rm up} = 125\ M_\odot$.

Initially all SPH particles get a temperature of 10^4 K, and all stars get an age of 300 Myr. At this age, the FUV flux of a stellar cluster has dropped below 1% of its maximum value. This assures an immediate cooling of the gas, but not too drastically. We let the simulations run for 1.5 Gyr. The results for the different runs are summarized in Table 2.2, where the first column gives the parameter that has been changed with respect to the default setting. The following columns give mean values for the interval 300 Myr $< t <$ 900 Myr (thus starting after a period of 300 Myr, so that the simulations have reached approximate equilibrium). Column 2 gives the star formation rate in $M_\odot$/yr for the whole galaxy, column 3 the total amount of cold gas, defined as having a temperature below 1000 K, and column 4 gives the amount of gas left at the end of the simulation.

Number of particles

Increasing the number of particles in steps of a factor 2 up to 40000/80000 SPH/star particles does not markedly influence the mean SFR and the total gas mass converted into stars. It has a small effect on the cold gas fraction due to the increased resolution: SPH particles can reach higher densities so that the cloud lifetimes become shorter, leading to less cold gas. However, since the free fall time goes with the square root of the density, this effect is not very large.

Given the consistency of SFR with number of particles we do not have to run very expensive calculations to test all parameters. Instead we feel safe in testing the recipe using 5000/10000 SPH/star particles, which takes about 60 CPU hours on a Sun SPARC20.

Cloud mass

M_c was chosen to be 10 times the mass of an individual SPH particle, with all SPH particles having the same mass initially. Eventually one would like to have a *number* for M_c, typically the size of a small GMC, say $10^5\ M_\odot$. But numerical problems can arise if M_c is chosen about equal to, or less than, the particle mass, since the smoothing over particles sets an upper limit to the maximum density that can be achieved.

As can be seen from Table 2.2, changing M_c up or down by a factor 4 does not have a significant effect on the SFR. This results from the two-phase structure of the ISM, which allows for stable warm and cold phases of the gas, but not for stable lukewarm gas. As long as the value of M_c implies an instability temperature well below that of the warm phase Eq.(2.7) essentially selects the same particles. This is demonstrated in Fig. 2.1, where the straight lines correspond to a Jeans mass equal to M_c. The two-phase structure of the gas is easily visible in this figure. For $M_c \leq 2.5 M_{\rm SPH}$ (Fig. 2.1e), problems with limited resolution start to appear.

Collapse time

The most influential model parameter is the collapse time for the cold gas particles, although its influence is still smaller than that of the IMF. If the collapse time is taken very small, essentially all regions that cool will produce stars rapidly, thus inhibiting the

TABLE 2.2— The results for various simulations of the model galaxy NGC6503. Only star formation parameters have been changed. The deviation from the standard setting is given in the first column.

Setting	SFR ($M_\odot$/yr) 300 Myr $< t <$ 900 Myr	$M_{\rm cold}$ ($10^9\ M_\odot$) 300 Myr $< t <$ 900 Myr	$M_{\rm gas}$ ($10^9\ M_\odot$) $t = 1.5$ Gyr
observations [a]	0.4		
standard	0.27	0.15	0.88
10,000/20,000 particles	0.25	0.14	0.88
20,000/40,000 particles	0.27	0.14	0.86
40,000/80,000 particles [b]	0.27	0.15	0.84
$M_c = 0.63\ 10^6\ M_\odot$	0.25	0.26	0.91
$M_c = 10.0\ 10^6\ M_\odot$	0.27	0.11	0.88
$t_c = 0.25 \times t_{ff}$	0.32	0.04	0.82
$t_c = 4.0 \times t_{ff}$	0.19	0.52	0.98
$\epsilon_{\rm SF} = 0.025$	0.26	0.25	0.90
$x = 0.01$	0.06	0.02	1.18
Miller-Scalo IMF [c]	0.21	0.09	0.99
Scalo IMF [c]	0.42	0.25	0.68
Salpeter IMF [d]	0.34	0.15	0.81
$\alpha = 1\ {\rm kpc}^{-1}$	0.43	0.36	0.57

[a] Kennicutt 1983 [b] $\epsilon_{\rm SF} = 1/30$ [c] $M_{\rm low} = 0.1\ M_\odot$, $M_{\rm up} = 125\ M_\odot$ [d] $M_{\rm low} = 0.1\ M_\odot$, $M_{\rm up} = 30\ M_\odot$

growth of the cold phase. If the collapse time is very large, it may effectively inhibit star formation. The dashed lines in Fig. 2.1 show the collapse time as function of density (time scale is plotted on the right axis). For the default recipe the collapse time is $20 - 100$ Myr for unstable particles, which corresponds roughly to the lifetimes of GMCs.

Figure 2.1f shows a simulation with an extremely long collapse time: over 1 Gyr. This leads to a high fraction of cold gas, almost no star formation (the simulation lasted only 1.5 Gyr) and a severe resolution problem. Such a choice for the collapse time is not realistic.

Star formation efficiency

Remarkably, the star formation efficiency $\epsilon_{\rm SF}$ does not influence the star formation *rate*, but it has some influence on the amount of cold gas. The formation of huge stellar clusters destroys the cold clouds efficiently, whereas smaller ones leave the clouds more nearly intact. In the standard simulation a new star particle has a mass of $2.5 \times 10^5\ M_\odot$, which is a bit large.

Ionization fraction

The recipe is very sensitive to the ionization fraction x assumed for the gas. Decreasing x from 0.1 to 0.01 depresses the SFR from 0.27 to 0.06 $M_\odot$/yr. This is due to the cooling properties of the gas, which are very sensitive to the ionization fraction. The cooling function at 10^4 K drops by a factor about 7 when x changes from 0.1 to 0.01. This means that the gas density must be higher by a factor 7 before it can start to cool, or, alternatively, less stellar heat input is required to keep the gas warm.

The ionization fraction is determined mainly by cosmic rays and soft X-rays, heating sources that we do not include in the calculations. Thus we have to adopt a value for x. A value of $x = 0.1$ seems reasonable for the solar neighbourhood (Cox 1990).

Initial mass function

The IMF directly controls the energy input from the stellar disk. Therefore our recipe should be very sensitive to it, and it is. In Fig. 2.2 we show the various IMFs used in our simulation, together with the FUV flux for each IMF (as given by Bruzual & Charlot 1993). If one integrates the FUV flux

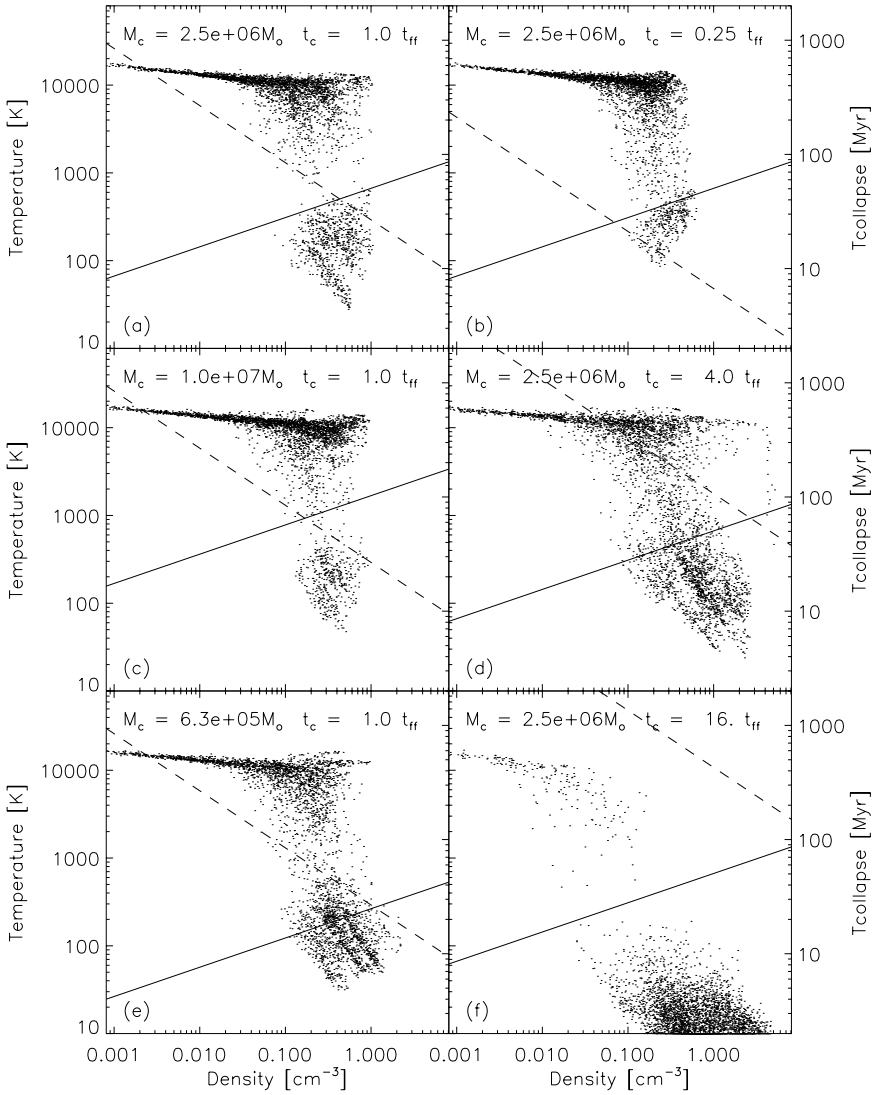

FIGURE 2.1— Diagnostic plots of temperature versus density in various simulations. Each dot indicates one SPH particle. The fully drawn line marks the Jeans mass corresponding to M_c, which is stated at the top at each panel together with the collapse time. The dashed line gives the collapse time versus density (the right axis shows the scale). The cold SPH particles have densities corresponding to the amount of heating: lowest density particles have lowest heating, highest density particles have highest heating (see also Fig. 2.10a where SPH particles are greyscale coded with the heating).

in time the total heat input from the stellar cluster is found. For mass cutoffs of $M_{\rm low} = 0.1\ M_\odot$, $M_{\rm up} = 125\ M_\odot$ one finds 5.0×10^{50}, 2.1×10^{50}, 7.2×10^{50} ergs/$M_\odot$ for Salpeter, Scalo and Miller-Scalo IMFs respectively, where this value is reached within about 10^9 yr. These differences in heat input are reflected directly in the SFR, which is lowest for the Miller-Scalo IMF (with highest energy input) and highest for the Scalo IMF (with lowest energy input). As is the case with the ionization fraction, the SFR does not scale linearly with the heat input, but has a weaker dependence. A Salpeter IMF with $M_{\rm up} = 30\ M_\odot$ gives a higher SFR, since the high mass stars contribute much to the FUV heating.

Absorption

One of the most difficult processes to include is the absorption of the FUV photons, since the gas column density between emitter and receiver of the photons has to be known: this is not easily solved in simulations of the type conducted here. Therefore we treat our galaxies as optically thin for FUV photons, thus setting an upper limit to the amount of dust heating of the ISM. In this respect the calculated SFR is a lower limit to the actual SFR.

To mimic the effects of absorption we run a simulation with an absorption coefficient of $1/\alpha = 1$ kpc. Thus the flux an SPH particle receives from a star particle declines not as $1/R^2$ but rather as $\exp(-\alpha R)/R^2$. This results

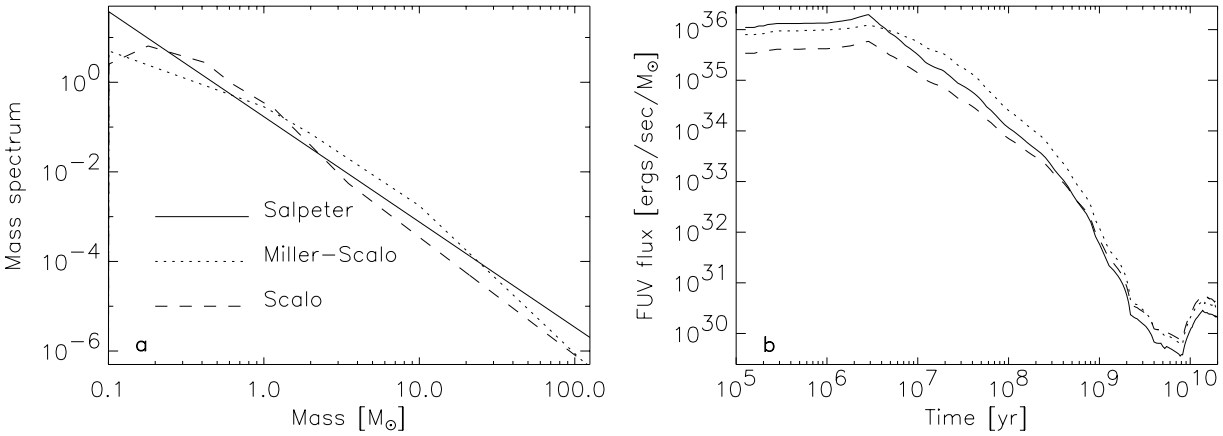

FIGURE 2.2— The frame on the left shows the mass spectrum for three different IMFs: Salpeter, Miller-Scalo and Scalo (straight, dotted, and dashed lines respectively), with mass limits of 0.1 and 125 $M_\odot$ as given by Bruzual & Charlot (1993). The corresponding FUV fluxes versus evolution time are shown in the frame on the right.

in a much higher SFR, since stars contribute only locally to the heating.

Summary

In summary we can say that the global star formation parameters resulting from our recipe are strongly dependent on physical input parameters, while only mildly dependent on model parameters. The cloud mass M_c has virtually no influence on the SFR or on the cold mass fraction. The collapse time has little influence on the SFR and cold mass fraction. The star formation efficiency has little influence on the cold mass fraction. The primary influence on the outcome of the simulations is the physical process of heating and cooling of the ISM. In our simplified model the heat input is controlled by the IMF (and the absorption), while the cooling is controlled by the ionization fraction.

2.2.3 Detailed analysis

In the previous section we discussed the global star formation rate and the cold gas fraction as a function of the input parameters. In this section we discuss one run in detail: the highest resolution simulation, which consists initially of 40,000 SPH particles and 80,000 star particles. The model is evolved using a time step of $\Delta t = 0.1$, using a tolerance parameter $\theta = 0.6$ and quadrupole moments to calculate the gravitational forces. The gravitational softening length for the particles is: $\epsilon = 0.02$. The hydrodynamic properties are calculated using variable smoothing lengths, such that each SPH particle has 32 neighbours within 2 smoothing lengths.

During the simulation, the energy and angular momentum of the galaxy were conserved to better than 0.2%. The simulation was performed on a Cray J32, and took 260 CPU hours.

For this simulation $M_c = 3 \times 10^5\ M_\odot$, $\epsilon_{\rm SF} = 1/30$, so newly formed star particles have a mass of $M_{new} \approx 10^4\ M_\odot$. Therefore this simulation has about the highest resolution one can obtain with our star formation recipe: *increasing the resolution must be accompanied with the input of new physics.*

Evolution

First we describe the global evolution of the galaxy. Recall that we do not start from scratch with a gaseous protogalaxy, but our initial conditions resemble a present-day galaxy. We focus on the SFR, the evolution of the various gas components, and show the correlation between the *total* gas mass and SFR.

In Fig. 2.3 the SFR is plotted against time. The SFR immediately rises to 0.3 $M_\odot$/yr and then remains constant at 0.27 $M_\odot$/yr. After

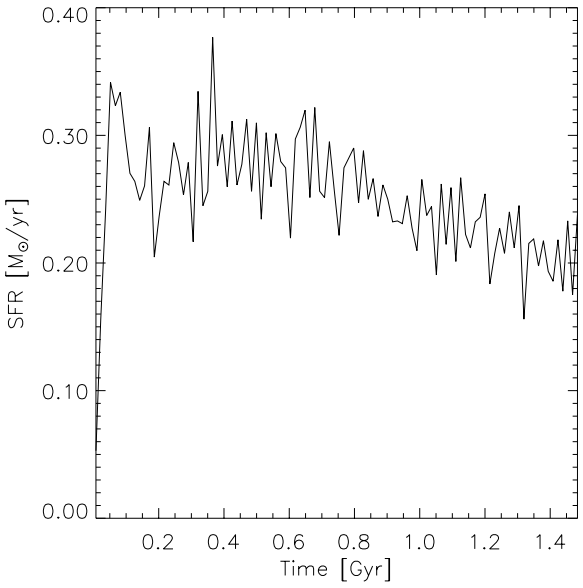

FIGURE 2.3— The star formation rate during the simulation. After settling of the system there is a slow decline of the SFR. The episodic changes in SFR are real and not due to limited resolution.

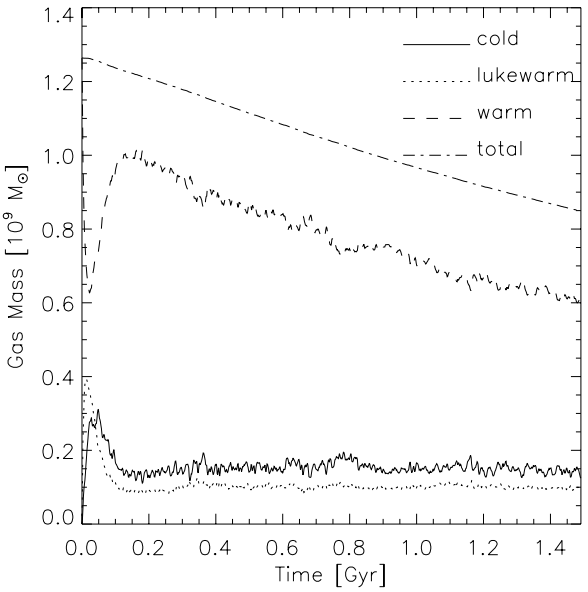

FIGURE 2.4— The global evolution of the gas. The dash-dot line shows the total gas, the fully drawn line the cold gas ($T < 1000$ K), the dotted line the lukewarm gas ($1000 \leq T \leq 8000$ K), and the dashed line shows the warm gas ($T > 8000$ K).

$t = 300$ Myr the SFR declines slowly. At this time all influence from the old stellar population, now 600 Myr old, has disappeared, and the SFR is completely determined by new stars. The episodic changes in SFR are probably real and due to the discrete nature of star formation. Only if the major mode of star formation would be in single stars, the global SFR could smear out to a single value.

Figure 2.4 shows the gas mass as function of time. Prominent in this figure is the approximately constant decline of the total gas mass, which reflects the rather constant SFR. The warm gas matches this decline perfectly, while the cold and lukewarm gas masses stay constant (here cold means below 1000 K). At the end of our simulation the gas mass contributes about 20% to the total galaxy mass, with 17% being cold. If we extrapolate this figure to a total gas mass of $0.4 \times 10^9\ M_\odot$, which is 10% of the galaxy mass, we would find that roughly half of the gas is in the cold phase.

Figure 2.5 shows the ratio of the SFR to the total gas mass versus time. This ratio is remarkably constant during the simulation, which suggests that *the total gas mass controls the global SFR of an isolated galaxy*. This explains the surprising observational result that the SFR correlates better with the total $\mathrm{HI} + \mathrm{H_2}$ masses than with the individual gas components (Ryder & Dopita 1994; Kennicutt 1989).

Spatial distribution

We now focus on the spatial distribution of the star formation and analyze the situation at $t = 900$ Myr. The initial stellar component has an age of 1.2 Gyr and will no longer influence the star formation other than gravitational.

Figure 2.6 shows the face-on and edge-on distributions of several components of the galaxy: (a) the old stellar component (the initial stellar disk), (b) the youngest stellar component (age under 150 Myr), (c) the warm gas, $T > 8000$ K, (d) the cold gas, $T < 1000$ K. There are two striking features in this plot. First there is the flocculent spiral structure in the cold gas and young stars and the *absence* of it in the warm gas and old stellar disk. Can we believe this spiral structure? In Fig. 2.7 the face-on cold gas is plot-

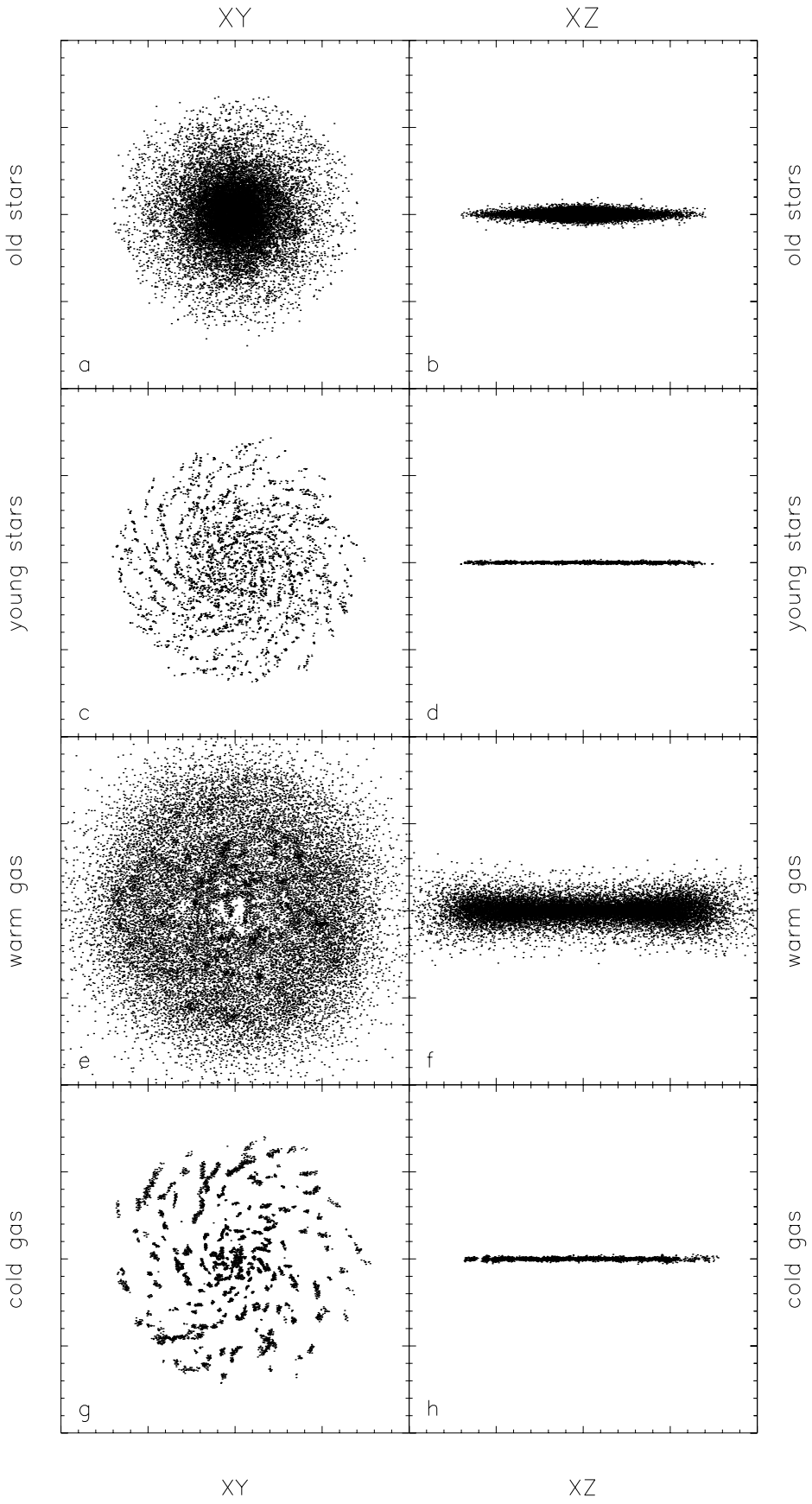

FIGURE 2.6— The particle distribution at $t = 900$ Myr. The left column shows the face-on distribution, the right column the edge-on distribution. From top to bottom are shown: the old stars, the young stars (younger than 150 Myr), the warm gas and the cold gas. The size of each box is 20×20 kpc. A random sample of at most 10000 particles is plotted.

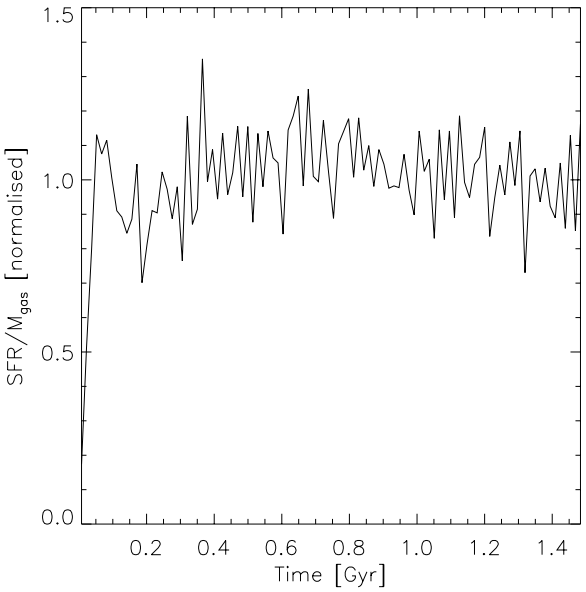

FIGURE 2.5— The evolution of the ratio of the star formation rate to the total gas mass.

ted again, now with four regions encircled. The characteristics of these regions are written in Table 2.3. From this table it is clear that the smallest group falls below our resolution of 32 particles, but the other groups are resolved and are candidates for real structures. Moreover, the same spirals already arise in the simulations presented in the previous section, with the same global appearance, so that they seem to be resolution independent. Still, our evolution movies show that these are transient structures, temporarily amplified by local processes, and are certainly not 'grand design' spirals. We expect to find those in our forthcoming work on interacting galaxies.

The second striking feature is that the cold gas and the young stars are confined to the plane of the stellar disk. It means that the gas can only cool sufficiently in the plane. In regions outside, the density is never high enough to allow cooling, or, conversely, the FUV radiation is strong enough to prevent cooling. This is in accordance with the observation that the scale height of young stars in the Milky Way is much smaller than for the old stars.

The radial distribution of the three gas components is shown in Fig. 2.8, where (a) shows the gas surface density against radius and (b) shows the relative gas distribution with radius. As can be seen from these figures most of the cold gas is in the centre of the galaxy (over 70% of the gas there is cold), while there is no cold gas outside 8 kpc.

TABLE 2.3— Cloud mass and extreme temperatures for the four cold cloud complexes encircled in Fig. 2.7. These are listed clockwise, starting with the lower one.

# of particles	$M_{\rm total}$ ($10^6\ M_\odot$)	$T_{\rm min}$ (K)	$T_{\rm max}$ (K)
72	1.8	38	867
39	1.0	58	612
337	8.8	28	930
18	0.4	176	776

The interpretation of the truncation of the cold disk, and consequently the truncation of the stellar disk, requires some care. Poor resolution effects at the edge of the galaxy may cause spurious results. Since the gas properties are always estimated by smoothing over 32 particles, SPH particles far out may have very large kernel lengths. Clumpy structures are improperly modeled in this regime, but may exist in reality and form stars. Another point of concern is that the observed H I disk for NGC6503 extends to 14.55 kpc, while we truncated it at 8 kpc. The outer gas thus lacks the pressure of the gas that should be surrounding it, so that it moves outward. The outermost gas particle at $t = 900$ Myr is 13.6 kpc away from the centre so the effect is indeed observed in the simulations. This leads to lower gas densities, which might inhibit cooling and contraction.

The final subject we discuss is the radial distribution of the new stars. In Fig. 2.9 we plot the surface density distributions of the young stars (fully drawn line) and the old stars (dotted line) in arbitrary units, scaled to fit in one plot. The decline of the surface density is slower for the young stars, which corresponds with the observed trend for spiral galaxies that the scale lengths are longer at blue wavelengths than in the red

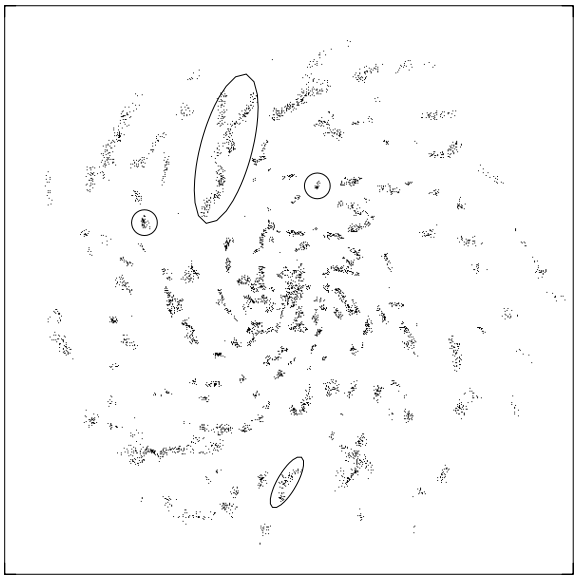

FIGURE 2.7— The cold SPH particle distribution at $t = 900$ Myr shown face-on. The characteristics of the four encircled regions are given in Table 2.3. The box has a size of 16×16 kpc.

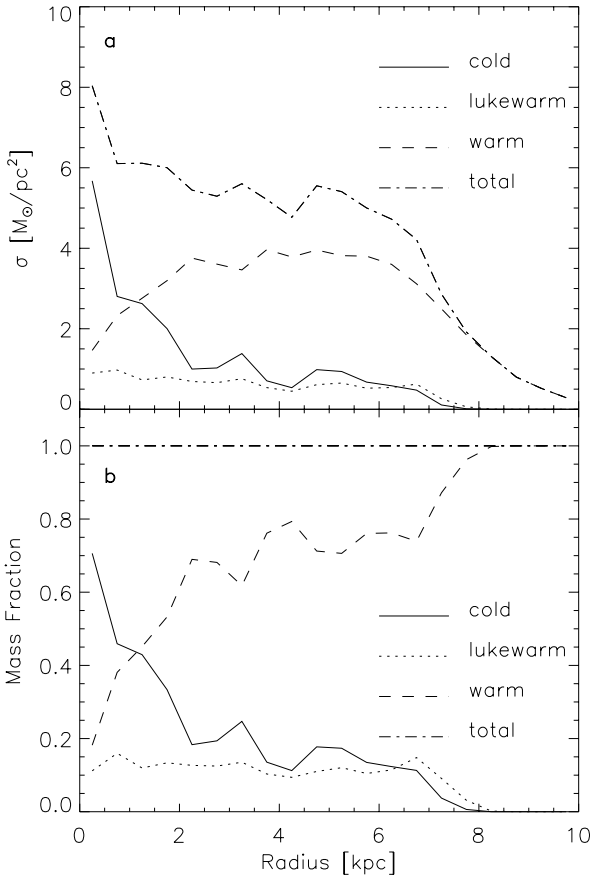

FIGURE 2.8— The spatial distribution of the gas. *a*: surface density of the various components; *b*: mass fractions occupied by these components. The dash-dot line represents the total gas, the fully drawn line the cold gas, the dotted line the lukewarm gas, and the dashed line the warm gas.

(De Jong 1996).

Recently Ryder & Dopita (1994) obtained photometric CCD imaging data for 34 spiral galaxies. From their I, V and Hα images they find a correlation between the surface brightness in the I-band (which measures the surface density of the old, low-mass stars, and this component determines the mass of a galaxy) and the Hα band: SFR $\propto \Sigma_I^{0.64\pm0.30}$. In a similar study Kennicutt (1989) found a correlation between the gas density and the Hα emission. Written as a Schmidt law the fit for his sample is: SFR $\propto \rho_{\rm gas}^{1.3\pm0.3}$.

The dashed line in Fig. 2.9 represents the Ryder & Dopita results for the stellar surface density, and the dot-dashed line shows the Schmidt law with exponent 1.3. The correlation of these two lines with the surface density of the young stars is striking. The physical reason of this correlation is discussed in §2.3.1.

Two-phase ISM

The first detailed description of the galactic ISM was the two-phase model of Field, Goldsmith & Habing (1969). Their model accounts for what we call the warm and cold gas, but not for the hot gas. Since our simulations do not include supernovae we do not get the three-phase model of McKee & Ostriker (1972), but the two phases are reproduced faithfully in our simulations.

In the standard two-phase model there is a limited range of thermal pressures for which there are two solutions for the gas density. Very low density gas is always warm, while very high density gas is always cold. In between the gas may be either. Starting with a warm, low density gas, one may increase the density until a certain fixed point. If the density is increased above that critical value the gas cools rapidly and will keep that low temperature when the density is increased

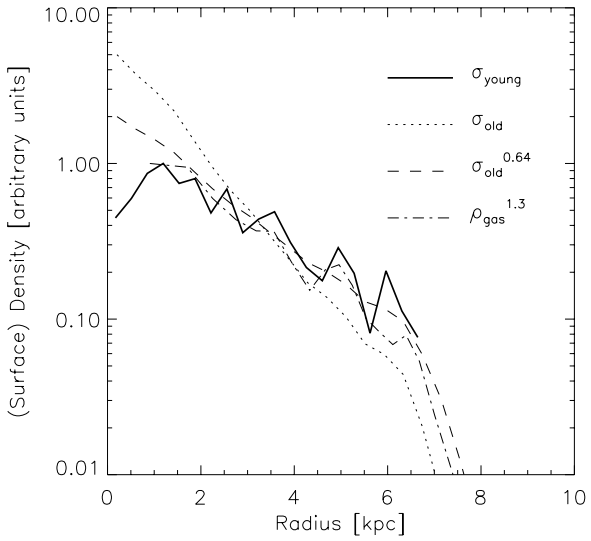

FIGURE 2.9— The spatial distribution of the young stars compared with that of the old. The thick line gives the young stellar surface density against radius, the dotted line shows the old stellar surface density, the dot-dash line shows Kennicutt's (1989) Schmidt law ($\rho_{\rm gas}^{1.3}$), and the dashed line gives the Ryder & Dopita (1994) fit for the star formation ($\sigma_*^{0.64}$). The (surface) densities are scaled to fit in one plot.

further (see e.g. Wolfire et al. 1995), as long as the heating rate is constant.

In our simulations the heating rate depends on position and time. This implies that the critical density is similarly dependent. This behaviour is shown in the two phase diagrams of Fig. 2.10. Figure 2.10a displays the density versus temperature, where the grey-scale coding denotes the heating rate. To one colour, meaning one heating rate, corresponds one critical density. If the density is lower than that, the gas is warm, while if the density is higher the gas is cool. The spread in heating rates thus explains the spread in density for the cold gas component.

Figure 2.10b shows the heating rate plotted against the pressure, where the grey-scale coding now denotes density. The gas particles that are plotted are all in the plane of the disk. The motion of the particles is illustrated in Fig. 2.11 and explained below.

Consider a particle at, say, $\log P = -3.0$ and $\log\Gamma = 1.0$ having a temperature of 10^4 K. If the density does not change, the particle only moves upward in the diagram if the heating increases, and downward otherwise. The latter happens if no stars form in the neighbourhood. The particle moves down (dotted line in Fig.2.11) until it reaches the sharp transition at $\log\Gamma \approx 0.3$ (indicated by the straight line). There the particle reaches its critical density (or critical heating). If the heating continues to decrease the particle cools rapidly to about 100 K and moves to the left in the diagram to $\log P \approx -4.5$. As long as no new stars form nearby the heating decreases steadily and the gas particle contracts with its neighbours to higher density and lower temperature, thus moving down and left. This process will stop if a new star is formed, which heats the gas, letting the gas particle jump to its original position (dashed line).

Interesting in this phase diagram is that we can immediately see why particles outside the galactic plane cannot cool. Particles outside the plane *only* occupy the region left of $\log P \approx -4$. These mostly move up and down in the diagram. The crucial point is that such particles cannot reach the line giving the critical heating (there is a gap between the particles and the line), so they will never be able to cool and collapse: no star formation can occur.

2.3 Discussion

The most prominent outcome of our simulations is the self-regulating character of the star formation. It is almost impossible to change the SFR unless one changes the gross physical properties of the parent galaxy. The explanation for the self-regulation is due to the star formation coupling back into the ISM, and can be viewed as thermal equilibrium of the ISM. If many stars form, the ISM heats up, the amount of cold gas declines, and the SFR must also decline. If only few stars form, the ISM cools down, the amount of cold gas increases and the SFR goes up. This effect has been discussed previously, e.g. in the chemo-dynamical models of Burkert, Truran & Hensler (1992).

Without additional constraints the simula-

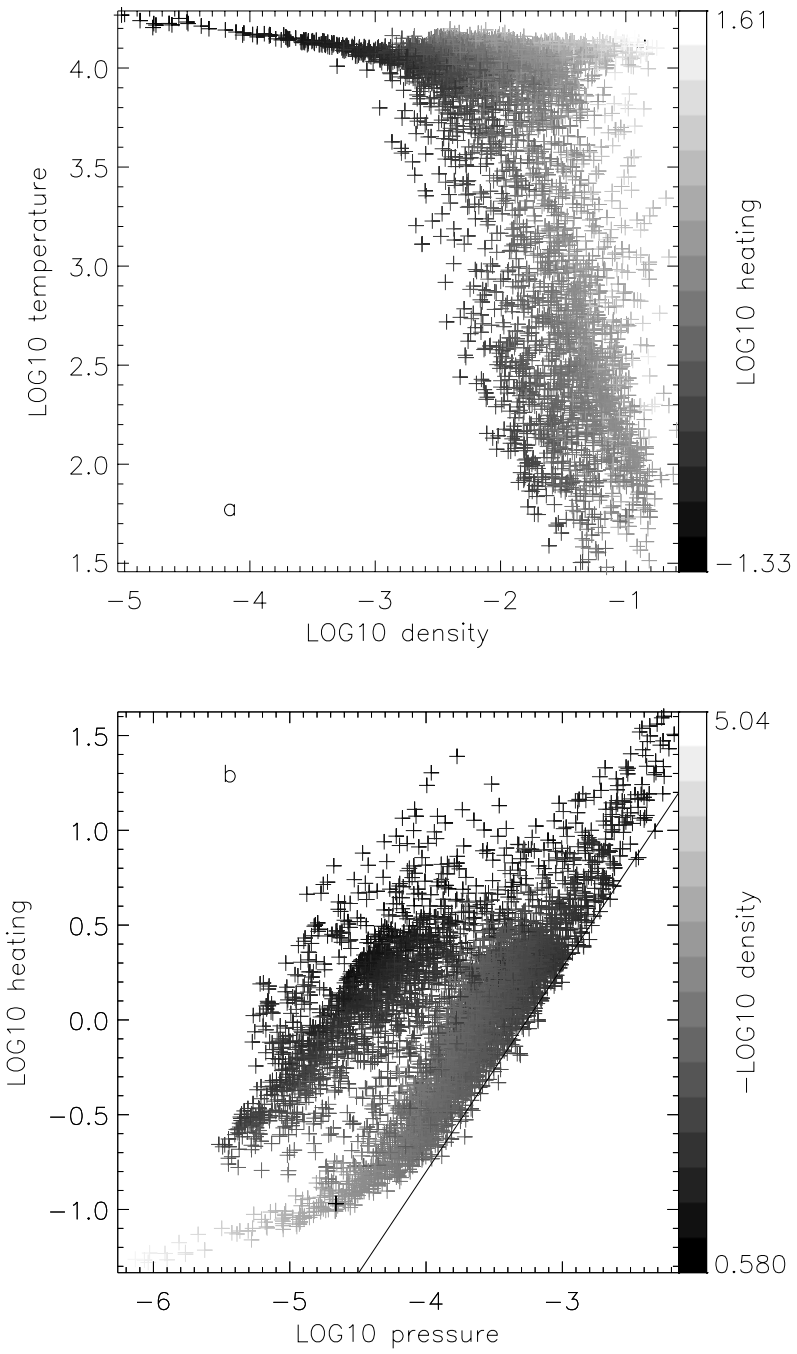

FIGURE 2.10— Phase diagrams for the SPH particles at $t = 900$ Myr. The upper diagram (a) shows temperature against density, while the grey-scale denotes the heating, black particles receive lowest heating, light grey particles receive most heating; the lower diagram (b) shows heating against pressure, where the grey-scale denotes the density, black particles have lowest density, light grey particles have highest density. The two-phase structure of the ISM is especially clear. The diagram only shows the particles in the plane of the galaxy. Those above and below the plane occupy the region of $\log P < -4$, and these particles are all warm.

tions produce a power law dependence of the SFR on the gas density, flocculent spiral arms and truncation of the stellar disk. The physical reasons for these processes are the following.

2.3.1 Schmidt law

Due to the self-regulation of the star formation the two major players in determining the SFR are the gas volume density and the heating rate. In a stellar disk that is much heavier than the gas disk the scale height of the gas (and hence its density) is completely determined by the stellar disk. Descriptions of the gas density for a gas layer embedded in an isothermal stellar disk can be found in e.g. Dopita & Ryder (1994) and Bottema (1996). If the z-density distribution is described by an exponential $\rho(z) = \rho_0 \exp(-z/z_0)$ the midplane velocity dispersion v_g of the gas is

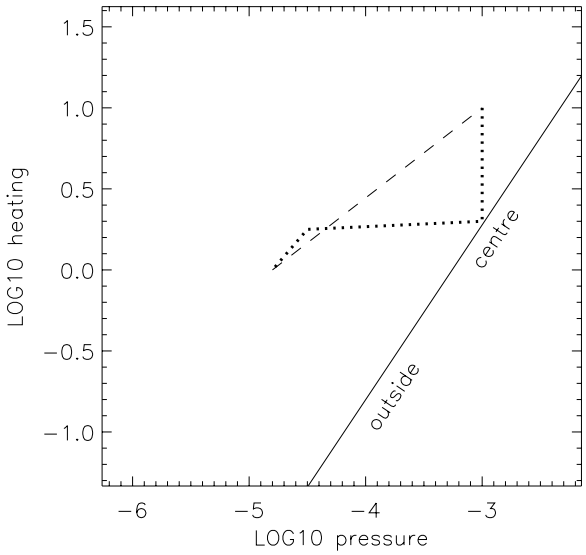

FIGURE 2.11— The motions of SPH particles in the phase diagram of Fig. 2.10b. The dotted line shows the trajectory of an SPH particle in the inner part of the galaxy. For particles farther away from the centre, the curve moves to the lower left in the diagram.

given by

$$v_g^2 = 2\pi G \sigma_T \frac{z_g^2}{z_* + z_g}, \qquad (2.17)$$

where σ_T is the total matter surface density (Dopita & Ryder 1994). In those regions where $\sigma_* > \sigma_g$ and $z_* > z_g$ (both conditions are true for our model galaxy within about 4 scale lengths), the gas density in the plane is approximated by

$$\rho_g = \left(\frac{2\pi G}{z_*}\right) \frac{\sigma_g}{v_g} \sigma_*^{0.5}. \qquad (2.18)$$

Observations of the velocity dispersion in external galaxies indicate that v_g is roughly constant among galaxies (Van der Kruit & Shostak 1984). Neutral hydrogen observations further show a variety of shapes of the H I surface density, but in general this is almost constant compared to the stellar surface density (see e.g. Cayatte et al. 1994). Together with the constant stellar scale height this implies $\rho_g \propto \sigma_*^{0.5}$.

The other component we have to know is the heating rate as function of radius. In the case of an optically thin ISM the heating rate is found by summing the contributions of all stars

$$\Phi_{\rm FUV}(\vec{r}) = \int_V \frac{\rho_*(\vec{r}\,')\,\phi}{\mid \vec{r} - \vec{r}\,' \mid} \, d\vec{r}\,', \qquad (2.19)$$

where ϕ is the FUV-flux/mass ratio. This integral cannot be solved analytically, but numerical integration shows that out to about 5 scale lengths the heating rate in the plane of the galaxy, resulting from a thin stellar disk, is well represented by

$$\Phi_{\rm FUV}(R) = \Phi_{\rm FUV}(0) \exp(0.75R/h_*). \qquad (2.20)$$

Accordingly, the heating rate declines as $\sigma_*^{0.75}$.

If there are no large gradients in the abundance of elements heavier than helium, the cooling properties of the gas are the same everywhere. Then in order to maintain thermal equilibrium, the radial dependence of the heating rate must equal the radial dependence of the gas density: $\sigma_*^{0.75n} \propto \sigma_*^{0.5}$, hence $n = 0.67$. For the SFR this implies that

$$\mathrm{SFR} \propto \sigma_*^{0.67} \propto \rho_g^{1.3}, \qquad (2.21)$$

in perfect agreement with the results of Ryder & Dopita (1994) and Kennicutt (1989).

2.3.2 Spiral structure

Now return to Fig. 2.6, and consider once more the flocculent spirals that are visible in the cold gas and young stellar disk. The lack of spiral structure in the old stellar disk means that the spiral structure in the cold gas is not due to a density wave. The structure must be due to the dissipational nature of the gas, which allows for clustering of the gas in large assemblies. The shear of the disk then causes the (trailing) spiral shape. The same conclusion about the origin of flocculent spiral structure has been reached by Elmegreen & Thomasson (1993) using 2D simulations.

The young stars also show this spiral structure since they form out of these cold spiral filaments. This is, in effect, the stochastic star formation mechanism (Seiden & Schulman

1990), with the physical driver being the molecular cloud complexes. Apparently there is no need for supernovae to stimulate star formation, although it might help to make the spiral structure more pronounced. Note, by the way, that this finding by no means excludes the usual swing amplification or density wave mechanisms for 'grand design' spirals, as we hope to show in our subsequent work.

2.3.3 Truncation

An interesting effect seen in the simulations is the sharp truncation of the cold gas disk and consequently of the young stellar disk. Truncation of galaxies is seen in edge-on galaxies, where the cut-off radii occur at about 4 radial scale lengths (Van der Kruit & Searle 1982; Bosma & Freeman 1993), while in our simulations this truncation occurs at approximately 6 scale lengths. The traditional explanation for truncation of a spiral galaxies invokes the angular momentum distribution of a collapsing protogalaxy, where the material with the highest specific angular momentum settles at a radius of about 4.5 scale lengths (Van der Kruit 1987).

Here we propose a thermal mechanism for the truncation. Although the interpretation in our simulations is complicated, it is interesting to see that the FUV radiation of the young stellar disk is capable of heating the entire gas disk. We can make a rough estimate of the conditions under which this effect could indeed prohibit star formation outside the stellar disk, using the radiation field and the gas density.

The radiation field outside the stellar disk declines with radius as $1/R^2$ due to geometrical dilution, where absorption is very unlikely to be important. The gas scale height h_g outside the stellar disk is determined by the halo and increases linearly with radius. If the gas is always warm, the density ρ must decrease at least as fast as the radiation field. Since $\rho = \sigma h_g$ this implies that the gas surface density σ should decline at least as $1/R$.

Note that we do not include any extragalactic radiation field in our simulations. Inclusion of such an external field requires less heat input from the stellar disk for heating the gas. Consequently the truncation will occur closer to the centre.

Abundance gradients may alter the situation greatly. If the gas outside the stellar disk is less enriched with heavy elements than the disk gas, it might be more difficult to heat the outer gas. On the other hand, this gas cools less efficiently. If the latter effect dominates, the requirement of a gas surface density which declines as $1/R$ can be relaxed, making truncation due to heating more likely.

2.4 Conclusions

Our approach to the inclusion of star formation produces galaxies that are similar to those observed, despite the limited amount of physics that has been put in. Effects that should be incorporated in the future are mass loss from stars in the form of supernovae and stellar winds, metallicity effects, ionization balance and a finite opacity.

Strong points of the recipe are its simplicity, the fact that it based on global properties (such as the Jeans criterion and radiative heating), the weak dependence on the model parameters and the strong dependence on the physical ingredients.

Our simulations produce self-regulated star formation due to thermal equilibrium of the ISM. They provide plausible explanations for flocculent spiral structure and truncation of galactic disks.

It is important to note that the TREESPH code does not require any special geometry. By its nature it is very well suited for three-dimensional problems such as interacting galaxies. We intend to run simulations of star formation in interacting starburst galaxies, simultaneously solving the complicated stellar radiation field, the highly inhomogeneous gas density and the dynamical heating. If we discard the dynamical heating the SFR should be approximately linearly correlated with the gas density in the starburst regions, since stellar heat input from outside is un-

important. Simulations of this kind will be presented in a future paper.

Acknowledgements

We are much indebted to Lars Hernquist for generously providing the TREESPH code, and to Teije de Jong and Peter Barthel for many stimulating discussions. We thank the referee for helping us to improve the paper. Our investigations were supported in part by the Netherlands Foundation for Research in Astronomy (NFRA) with financial aid from the Netherlands Organization for Scientific Research (NWO).

References

Barnes J., Hut P., 1986, Nature 324, 466
Barnes J.E., Hernquist L., 1991, ApJ 370, L65
Binney J., Tremaine S., 1987, *Galactic Dynamics* (Princeton: Princeton Univ. Press), 1
Blaauw A., 1991, in *The Physics of Star Formation & Early Stellar Evolution*, eds. Lada C.J., Kyfalis N.D. 125
Bodenheimer P., 1992, in *Star Formation in Stellar Systems*, eds. Tenorio-Tagle G., Prieto M., Sánchez F. (Cambridge University Press), 3
Boselli A., Gavazzi G., Lequeux J., et al., 1995, A&A 300, L13
Bosma A., Freeman K.C., 1993, AJ 106, 1394
Bottema R., 1989, A&A 221, 236
Bottema R., 1993, A&A 275, 16
Bottema R., 1996, A&A 306, 345
Bottema R., Gerritsen J.P.E., 1997, MNRAS 290, 585
Bruzual B.A., Charlot S., 1993, ApJ 405, 538
Burkert A., Truran J.W., Hensler G., 1992, ApJ 391, 651
Cayatte V., Kotanyi C., Balkowski C., Van Gorkom J.H., 1994, AJ 107, 1003
Cox D.P., 1990, in *The Interstellar Medium in Galaxies*, eds. Thronson H.A., Shull J.M. (Kluwer: Dordrecht), 181
Dalgarno A., McCray R., 1972, ARA&A 10, 375
De Jong R.S., 1996, A&A 313, 377
Dopita M.A., Ryder S.D., 1994, ApJ 430, 163
Elmegreen B.G., 1992, in *Star Formation in Stellar Systems*, eds. Tenorio-Tagle G., Prieto M., Sánchez F. (Cambridge University Press), 3
Elmegreen B.G., Thomasson M., 1993, A&A 272, 37
Field G.B., Goldsmith D.W., Habing H.J., 1969, ApJ 155, L149
Friedli D., Benz W., 1995, A&A 301, 649
Gingold R.A., Monaghan J.J., 1977, MNRAS 181, 375
Habing H.J., 1968, Bull. Astron. Inst. Netherlands 19, 421
Hernquist L., 1987, ApJS 64, 715
Hernquist L., 1989, Nature 340, 687
Hernquist L., Katz N., 1989, ApJS 70, 419
Katz N., 1992 ApJ 391, 502
Katz N., Gunn J.E., 1991, ApJ 377, 365
Katz N., Weinberg D.H., Hernquist L., 1996, ApJ 105, 19
Kennicutt R.C., 1983, ApJ 272, 54
Kennicutt R.C., 1989, ApJ 344, 685
Knapp G.R., 1990, in *The Interstellar Medium in Galaxies*, eds. Thronson H.A., Shull J.M. (Kluwer: Dordrecht), 3
Lucy L.B., 1977, AJ 82, 1013
McKee C.F., Ostriker J.P., 1977, ApJ 218, 148
Mihos J.C., Hernquist L., 1994, ApJ 437, 611
Navarro J.F., White S.D.M., 1993, MNRAS 265, 271
Ryder S.D., Dopita M.A., 1994, ApJ 430, 142
Schmidt M., 1959, ApJ 129, 243
Seiden P.E., Schulman L.S., 1990, Adv. Phys. 39, 1
Shu F.H., Adams F.C., Lizano S., 1987, ARA&A 25, 23
Van der Kruit P.C., 1987, A&A 173,59
Van der Kruit P.C., Searle L., 1982, A&A 110, 61
Van der Kruit P.C., Shostak G.S., 1984, A&A 134, 258
Van Dishoeck E.F., Black J.H., 1986, ApJS 62, 109
Wolfire M.G., Hollenbach D., McKee C.F., Tielens A.G.G.M., Bakes E.L.O., 1995, ApJ 443, 152